Geophys. Astrophys. Fluid Dynamics, 2002, Vol. 96, No. 3, pp. 223–238

NONMODAL GROWTH ON A SPHERE AT VARIOUS HORIZONTAL SCALES

RICHARD GROTJAHN* and CRIS CASTELLO

Atmospheric Science Program, Department of Land, Air, and Water Resources, University of California, Davis, CA 95616 USA

(Received 24 August 2001; In final form 21 December 2001)

Nonmodal growth (NG) and unstable normal mode growth are considered in spherical geometry. Two groups of initial conditions (IC) are studied: "connected" IC (common in Cartesian studies) and "separated" IC (based on observed conditions prior to cyclogenesis). Time series of growth rates are emphasized in conjunction with eigenmode projections.

Projections show that early on normal mode growth was much stronger for connected IC and that NG caused negative growth early on of some variables for separated IC. Projections explain why amplitude, kinetic energy (KE), and potential vorticity have more NG than available potential energy (APE).

Though varying between ICs and with initial phase shift, NG increases with wavenumber. For middle wavelengths, NG is significant and positive using connected IC but negative or small using separated IC. Total energy and KE growth rates of short waves are very similar during the first 2 days for both ICs. Amplitude time series closely follow KE in all cases studied. APE has less overlap than does KE between the main modes present, so less NG occurs for APE than for KE. In separated IC cases, APE growth rates evolve consistent with emergence of an unstable normal mode and little NG.

Keywords: Baroclinic instability; Nonmodal growth; Spherical coordinates

1. INTRODUCTION

This paper examines the relative importance of nonmodal growth (NG) and unstable normal mode growth (UNMG) in spherical geometry. NG may be understood as increasingly favorable superposition of constituent eigenmodes traveling at different speeds (e.g. Hodyss and Grotjahn, 2001). For UNMG, the unstable eddy has a precise structure that is maintained during growth. In contrast, eddy structure in one or more dimensions varies during NG. One does not expect atmospheric eddies to start growth with the precise structure of an UNMG eigenfunction. However, while NG can be very large for an optimally chosen initial condition (IC) most IC will not optimize NG and realistic ones may actually have little NG (Grotjahn and Tribbia, 1995; Hodyss and Grotjahn, 2001).

*Corresponding author. Dept. of L.A.W.R., One Shields Ave., UCD, Davis CA 95616, USA. E-mail: grotjahn@ucdavis.edu

ISSN 0309-1929 print: ISSN 1029-0419 online
DOI: 10.1080/03091920290011003

The NG mechanism has been studied by a variety of researchers during the past two decades. Prior work on NG has emphasized: the dynamics of the process (e.g. Farrell, 1984); optimal structure (Farrell, 1989); how NG varies with initial state (e.g. Grotjahn *et al.*, 1995; Grotjahn and Tribbia, 1995); the structure at peak growth (e.g. O'Brien, 1992); and other factors. The prior work often treats the meridional structure in a simple way (for example, by assuming no meridional variation). NG might be identified by default when no other source of growth is present as when the initial state is constructed entirely neutral modes (e.g. Rotunno and Fantini, 1989). Typically, instantaneous growth rate time series are used to identify periods where the instantaneous growth rate exceeds the largest rate of the normal modes present (e.g. Whitaker and Barcilon, 1992, for a linear model; Rotunno and Bao, 1996, for nonlinear models); though as discussed below, considerable care is needed. Recently, Hodyss and Grotjahn (2002) extended prior work to focus on how NG varies with the horizontal scale and by using a model having fewer approximations than the popular Eady (1949) model. (Badger and Hoskins, 2001, consider a few different horizontal scales in the Eady model.) In this study, we look at the influence of spherical geometry upon the relative importance of NG and UNMG for a realistic mean flow and IC at various zonal wavelengths. The model and IC are described in the next section followed by a presentation of representative results and conclusions. The abbreviations used are summarised in the Appendix.

2. EXPERIMENTAL METHODOLOGY

2.1. Overview

A linear, quasi-geostrophic (QG) spherical, spectral model based on Hollingsworth, *et al.* (1976) is solved as an eigenvalue problem and as an initial value problem. The eigenvalue problem provides normal mode growth rates and phase speeds that we compare to similar models and use to diagnose the initial value results. The initial value problem is used to study the development of NG in two different types of ICs: a "connected" vertical structure and a "separated" vertical structure. The connected IC is an analog to ICs commonly used in most prior work in Cartesian geometry. The connected IC develops large NG in Cartesian models, especially simpler models like Eady's (see comparison in Hodyss and Grotjahn, 2001). The separate IC is intended to approximate conditions prior to observed cyclogenesis (e.g. Grotjahn, 1996). In Cartesian models, the separated IC has much less NG for most global parameters. Both initial conditions are run with varying amounts of vertical offset (upstream tilt). This study emphasizes how the relative amounts of NG vary using differing amounts of vertical offset for each of the two initial conditions, and how the NG results compare to those in similar Cartesian geometry models.

2.2. Model Formulation

The model governing equation, representing conservation of QG potential vorticity (QGPV), is developed following Hollingsworth, *et al.* (1976). The model governing equation consists of non-dimensional, linearized conservation of QGPV. The non-dimensionalization is made following Frederiksen (1978) where a (the Earth's radius)

is the length scale, Ω^{-1} (inverse of earth's angular velocity) is the time scale, $a\Omega$ is the velocity scale, $a^2\Omega^2/R$ (R is the gas constant) is the temperature scale, and 1000 hPa is the scale for p (pressure). In the interior of the domain, the governing equation is

$$\frac{\partial q}{\partial t} = \frac{\partial \bar{\psi}}{\partial \mu}\frac{\partial q}{\partial \lambda} - \frac{\partial \psi}{\partial \lambda}\frac{\partial \bar{q}}{\partial \mu} + \frac{\partial \psi}{\partial \lambda}\left[8\mu \frac{\partial}{\partial p}\left(\frac{p}{\sigma}\frac{\partial \bar{\psi}}{\partial p}\right)\right], \tag{1}$$

where q is the perturbation QGPV, $\bar{q}$ is the basic state QGPV, ψ is the perturbation streamfunction, $\bar{\psi}$ is the basic state streamfunction, μ is sine of latitude, λ is longitude, p is pressure, and σ is the static stability parameter $(-T/\theta)\,\partial\theta/\partial p$, where θ is potential temperature and T is temperature. In the interior of the domain, q and $\bar{q}$ are defined as follows:

$$q = \nabla^2\psi + 4\mu^2\frac{\partial}{\partial p}\left(\frac{p}{\sigma}\frac{\partial \psi}{\partial p}\right),$$
$$\bar{q} = \nabla^2\bar{\psi} + 4\mu^2\frac{\partial}{\partial p}\left(\frac{p}{\sigma}\frac{\partial \bar{\psi}}{\partial p}\right) + 2\mu.$$

Assuming no vertical motion at the top and bottom boundaries, we obtain alternate definitions of q and $\bar{q}$ to still satisfy (1). At the bottom boundary q and $\bar{q}$ are (subscripts indicate vertical levels, 1 being the bottom level):

$$q = \nabla^2\psi + \frac{8\mu^2 p_1}{\sigma(p_2 - p_1)^2}(\psi_2 - \psi_1),$$
$$\bar{q} = \nabla^2\bar{\psi} + \frac{8\mu^2 p_1}{\sigma(p_2 - p_1)^2}(\bar{\psi}_2 - \bar{\psi}_1) + 2\mu.$$

At the top boundary, q and $\bar{q}$ are

$$q = \nabla^2\psi + \frac{8\mu^2 p_{\mathrm{Top}}}{\sigma(p_{\mathrm{Top}} - p_{\mathrm{Top}-1})^2}(\psi_{\mathrm{Top}-1} - \psi_{\mathrm{Top}}),$$
$$\bar{q} = \nabla^2\bar{\psi} + \frac{8\mu^2 p_{\mathrm{Top}}}{\sigma(p_{\mathrm{Top}} - p_{\mathrm{Top}-1})^2}(\bar{\psi}_{\mathrm{Top}-1} - \bar{\psi}_{\mathrm{Top}}) + 2\mu.$$

The model uses eight vertical levels, equally spaced in pressure coordinates. The bottom level is at 1000 mb, the top level at 100 mb. Parallelogramic truncation is used to truncate the spherical harmonics. Parallelogramic truncation is similar to rhomboidal truncation, except that the numbers of zonal and meridional harmonics kept in the calculations are not the same. For the initial value problem, P20/30 truncation is used. P20/30 keeps 21 zonal wavenumbers (0 through 20) along with 31 meridional waves at each of the zonal wavenumbers. For the eigenvalue problem, P10/30 is used to keep computational needs within the capacity of the available computer.

2.3. Basic State and Initial Conditions

In order to compare results from previous spherical models we choose basic state zonal wind and temperature profiles used by Simmons and Hoskins (1976) and Frederiksen (1978). Specifically, we use a zonally averaged basic state consisting of an internal jet centered at 30° latitude. The 30° jet and the mean temperature profile are both defined by a polynomial fit to five prescribed values following Simmons and Hoskins (1976, p. 1458) Details can be found in Appendix B of the Frederiksen paper. The model is run as an eigenvalue problem to identify normal mode structures, growth rates, and phase speeds. Eigenvalue problem results were very similar to the results described in Frederiksen (1978), who used a similar (but not identical) spherical model. Fig. 1(a) in Frederiksen (1978) compares growth rate curves between his QG model, the QG model used in Simmons and Hoskins (1976), and a primitive equation (PE) model. Growth rate results for our model were indistinguishable from Frederiksen's PE curve, giving us confidence that our model was capturing enough of the essential

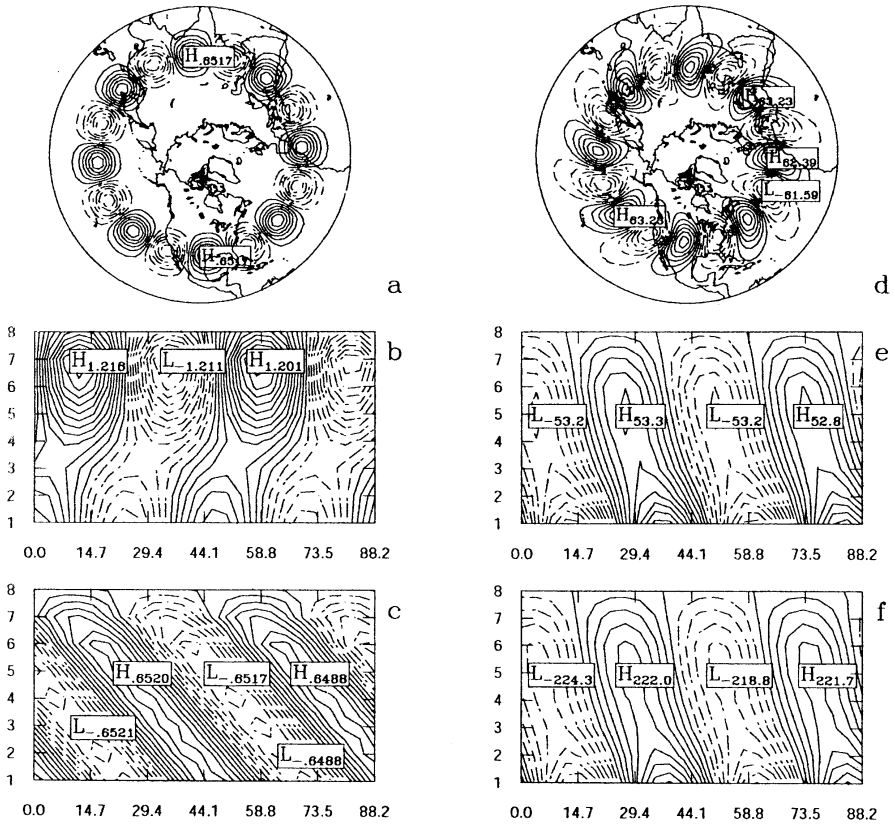

FIGURE 1 Separated and connected cases initial conditions (left column) for rm = 1.5 and $k = 8$. (a) Structure at bottom surface. (b) Zonal cross section at 30 N for the separated IC; (c) for the connected IC. (d)–(f) same as corresponding (a)–(c) except after four days. Dashed lines are used for negative values. The contour interval varies between plots.

physical processes. Using their parameter values, the zonal wind in the center of the jet reaches a speed of ~45 m/s and the fastest growing modes were found to occur at horizontal wavenumbers 8 and 9, with growth rates near 0.6/day.

Examples of the connected and separated initial states are shown in Figs 1(a)–(c). The horizontal structures of the initial states are shown, in this case for wavenumber 8. Note that the meridional structures of the initial conditions contain one peak near 30°N and tail off towards the pole and equator. The meridional structure uses a Gaussian profile such that the meridional scales of individual highs and lows approximately match the zonal scale. This matching recognizes that most observed frontal cyclones have similar zonal and meridional scale in the geopotential height fields (e.g. Grotjahn and Castello, 2000). These examples illustrate a tilt represented by a $3\pi/2$ phase shift between the top and bottom model levels. Three different phase shifts were tested with the connected initial state and run as individual cases: a $\pi/2$ phase shift, a π phase shift, and a $3\pi/2$ phase shift. Two different phase shifts are emphasized for the separated initial state: a π phase shift and a $3\pi/2$ phase shift.

Grotjahn *et al.* (1995) examined cases similar to our connected cases, for varying amounts of initial upstream tilt. That study found that the degree of tilt had little effect on the peak growth rate although larger upstream tilts delayed the time of the peak growth rate. The construction of the separated initial condition is motivated by results from Grotjahn (1996). Twenty-seven extratropical cyclones were tracked before and during cyclogenesis near the east coast of Asia. These cyclones formed when an upper trough moved sufficiently close to the surface trough, similar to "type B" cyclogenesis (Pettersen and Smebye, 1971). The upper and lower troughs were unconnected and each had no upstream tilt. The separated initial condition used in this study is intended to represent this observed condition.

2.4. Diagnostic Parameters

The diagnostics used in this study are defined as follows (ϕ is latitude):

$$\mathrm{KE} = \frac{1}{2}\int\int\left[\left(\frac{\partial\psi}{\partial\mu}\cos\phi\right)^2+\left(\frac{\partial\psi}{\partial\lambda}\frac{1}{\cos\phi}\right)^2\right]dA\,dp, \quad \mathrm{APE} = \frac{1}{2}\int\int\left(\frac{\partial\psi}{\partial p}\right)^2\frac{4\mu^2 p}{\sigma}\,dA\,dp,$$

$$\mathrm{TE} = \mathrm{APE} + \mathrm{KE}, \quad \mathrm{L2} = \frac{1}{2}\int\int\psi^2 dA\,dp, \quad \mathrm{H} = \frac{1}{2}\int\int q^2 dA\,dp.$$

Due to the power of two in all of these diagnostics, they will asymptote to twice the growth rate of the most unstable normal mode (MUNM) for the particular zonal wavenumber.

In studies using localized initial states (Simmons and Hoskins, 1979; Whitaker and Barcilon, 1992; Grotjahn *et al.*, 2002; etc.) growth rates of the peak value at some level are tracked instead of a global parameter because each high and low behaves differently. Since they behave differently and may change shape over time, the domain for each integral in the diagnostics listed above would be arbitrary. In contrast, the growth is uniform in this study and global integrals work well. As a further test, we explored using different meridional ranges and found no material effect upon the results.

The relative presence of NG or UNMG is identified using time series of the growth rates of amplitude norm (L2) and mass-integrated total energy (E) and potential

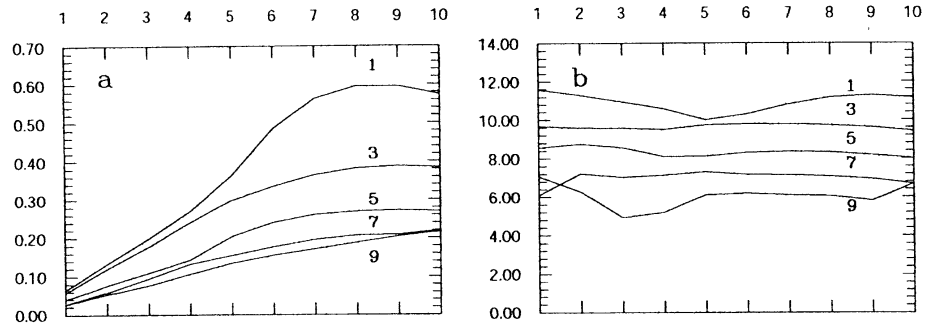

FIGURE 2 (a) Growth rates (in day^{-1}) and (b) phase speed (in m/s) for the top five most unstable equatorially symmetric normal modes for the 30 N jet with peak velocity of 45 m/s. The abscissa is zonal wavenumber. Each symmetric mode has a similar antisymmetric counterpart. Labels on curves are 2 UMR-1 for these top five symmetric modes.

enstrophy (H). The E parameter is further subdivided so as to understand better the source of the NG. Instantaneous growth rates can exceed the normal mode rate only by the NG mechanism in this model. Over time, the growth rates asymptote to that of the MUNM values. If the IC is purely a growing normal mode, then the growth rates immediately equal that of the normal mode. An IC can have little or no NG if the modes present move at about the same phase speed (or have little overlap); if the IC also contains one or more growing normal modes, then the growth rate of the total solution will ramp up to the normal mode value similar to the H′ curves in Fig. 2 of Grotjahn and Tribbia (1995). How quickly the growth rates approach 95% (say) of the normal mode value depends on how quickly the most unstable mode dominates the solution. (Several factors affect the timing: relative amounts of the modes present, the differences between their growth rates, etc.) One may assess what fraction of the current state is due solely to the MUNM by projecting the total solution onto the MUNM and comparing that with what remains when that projection is subtracted out. Grotjahn and Tribbia (1995) do this. Using such projections to partition growth into UNMG and NG parts becomes ambiguous when there is more than one normal mode having a growth rate similar to that of the MUNM. In our spherical coordinates model, the middle waves (e.g. zonal wavenumbers 5–10) have second and third most unstable modes with growth rates about two thirds and one half of MUNM growth rates. For example, at wavenumber 8, the three most unstable symmetric modes growth rates are 0.595, 0.382, and 0.269. (The eigenfunctions often occur in equatorially symmetric and antisymmetric pairs for the symmetric basic flow. However, only the symmetric member of each pair has any appreciable projection during the time integrations made). So, we can adopt a simple procedure of testing the instantaneous state for the amount of MUNM present. Based in part on our past experience with simpler problems, when the MUNM exceeds 90% of the total, observed growth is assumed dominated by the UNMG mechanism. When the projection is large onto the MUNM, growth rates will ramp up to a value that is close to the UNMG rate and this situation likely has comparatively little NG. Growth rates for the separated IC evolve in this fashion and so they are dominated by the UNMG mechanism. Situations which exceed the UNMG rate, particularly during the first few days of simulated time are

ones having comparatively large NG. With this general interpretation, it will be found that the connected IC can have significant growth during the first few days dominated by the NG mechanism.

3. RESULTS

3.1. Eigenfunction Overview

The 8 layer P10/30 eigenvalue problem has 311 growing normal modes and an equal number of decaying modes. Almost half of each are symmetric with respect to the equator. The remaining 2296 modes are labeled "continuum modes" by analogy with the continuous spectrum. The continuum modes have zero growth rate. For each nonzero wavenumber ($k > 0$) there are 256 modes, half of which are symmetric. At wavenumber 8, there are 34 growing modes. Only symmetric modes are discussed.

The growth rate spectrum for the MUNMs (unstable normal mode rank, UMR = 1) has a broad maximum with largest growth rate at zonal wavenumber, $k = 9$ and an essentially equal peak growth rate at $k = 8$ (Fig. 2a). The second most unstable modes (UMR = 2) have similar growth rate for $k < 5$ but about half the peak rate for $k = 7$–10. Fig. 2(a) shows curves for UMR = 2–5; each of these UMR curves peaks at a wavenumber, $k > 8$.

For the five most rapidly growing modes, phase speed generally increases for increasing instability, i.e., as UMR decreases (Fig. 2b). The most unstable modes (UMR = 1) have speeds ~ 11 m/s while the UMR = 5 modes have speeds ~ 6 m/s. The phase speed for an unstable mode of a given UMR is nearly constant with wavenumber. This result may have implications for localized structures: as the MUNM emerges at each k, for a localized structure, they will move together and little NG would be possible from these most unstable symmetric modes.

The horizontal structure varies considerably between the five most unstable modes at a given zonal wavenumber. Only the Northern Hemisphere is discussed here. The UMR = 1 mode is monopole; it has a single dominant maximum in the meridional direction. The location of the maximum (the central axis) is near 37°N for $k = 4$, 8, and 10. The UMR = 2 mode at these wavenumbers is a dipole mode (two extrema in the meridional direction). The extrema are near 30 and 45°N. The UMR = 3 mode has three extrema along a meridian; however, at $k = 4$ these result from two wavetrains, the more poleward one being zonally elongated with a WNW to ESE horizontal tilt. These tilts imply equatorward momentum flux by the higher latitude chain of eddies. For $k = 4$, the more poleward chain has larger amplitude; the location varies with UMR; for UMR = 3, 4, and 5 peak amplitude occurs near 46, 48 and 55°N. However, all of the five most unstable modes at $k = 4$ have significant amplitude near 30°N. There is some tendency for the upstream tilt with height to diminish for less unstable modes at $k = 4$. At $k = 8$, the number of extrema between equator and pole equals UMR; at $k = 10$ the number of extrema equals UMR for UMR < 5.

The vertical structure shows upstream tilt with height when a zonal cross section is made at the latitude where the surface amplitude is largest. At $k = 4$, the tilt diminishes as UMR increases from 3 to 5 and all of the top five modes have a similar upper level maximum that is about 2/3 the surface magnitude. These modes look more like the most unstable normal modes found in Cartesian geometry. At $k = 8$ and 10, the

upstream tilt is nearly identical for the top five modes, however, the modes become more bottom trapped as UMR increases. These modes do not have a discernible upper level maximum and seem like "short waves" solutions in Cartesian geometry where they would have much slower growth.

It has been suggested[1] that the track of the most unstable mode may be much further poleward for weaker jet profiles. The 30° jet used by us and the prior authors listed above has maximum wind speed of ~45 m/s. We consider two weaker jets to test this idea. We use a constant multiplier giving 30 and 15 m/s peak wind speeds. The primary differences are these. The phase speeds decrease by a greater amount than the maximum wind speed. Phase speeds for the 30 m/s jet are about half that of the 45 m/s jet and about three times that of the 15 m/s jet. In all three cases the phase speeds have comparatively small variation with wavenumber for the more unstable modes. The peak growth rate decreases with the same proportion as the peak jet speed. However, the growth rates of longer waves decrease much more rapidly than the change in peak jet speed. One consequence is that the growth rates peak at higher wavenumber as the speed decreases. The difference between growth rates for UMR = 1 and 2 also shrinks as the jet speed decreases; for example, the 15 m/s jet with $k = 8$ has top growth rates of 0.020 and 0.019. Consequently, it would be more difficult to separate NG and UNMG in the way done here for these slower basic jets. We do not find any evidence for a poleward shift of the wavetrain. For all three basic states, the most unstable mode has peak amplitude along the 39.1°N Gaussian latitude.

3.2. Structural Changes Over Time

Evolution of the wave #4 structure implies poleward momentum flux for both ICs. These WSW to ENE tilts develop sooner and are stronger for the separated IC cases. The wavetrain remains centered at 30–28°N: on or near the axis of the basic state jet. The lower maximum grows faster than the upper maximum as the normal mode structure emerges (upper becomes ~60% of the surface maximum). Because NG is stronger, the connected case (rm = 1.5) has about three times the amplitude of the separated case for days 6 and after.

The wave #8 structure develops horizontal tilts (Fig. 1(d)) indicative of eddy momentum convergence centered to the North of the basic state jet axis. The wavetrain migrates poleward of the basic state jet: by day 8 it is 5–7°N. The upper level amplitude becomes about half the surface amplitude. The structures evolving from both ICs are broadly similar by day 3 and very similar by day 6. Because of the greater NG, the connected case solution (rm = 1.5) has about four times greater amplitude during days 4 and after (visible in Figs. 1e and f.)

For wave #12, little horizontal tilt develops; there is perhaps a slight poleward eddy momentum flux present on the equatorward side of the eddies. However, the eddies are centered ~8 degrees poleward of the basic state jet axis. Upper level development is very small, as the growing normal modes are strongly bottom-trapped. The eddy amplitude decreases to 1/e of the surface value before 600 hPa elevation is reached. The connected

[1]Personal communication, Lee, Sukyoung and Kim, H.-K. (2001) "On the relationship between subtropical and eddy-driven jets." Poster presented at 13th Conference on Atmospheric and Oceanic Fluid Dynamics. Breckenridge, Colorado, USA.

and corresponding separated solutions are broadly similar by day 5 and very similar by day 8. The greater NG makes the connected case amplitude about four times the separated case amplitude by days 4 and after.

3.3. Total Energy Growth Rates

For the connected case, the peak TE growth rate increases with wavenumber (Fig. 3a). The growth rate for $k=20$ exceeds 2. As the phase shift is increased, the peak values diminish for middle wavelengths ($k=4$–10). The peak growth rate at $k=8$ is almost 1.3 times the asymptote (peak instantaneous over asymptotic growth rates ratio, GRR = 1.3). The time that peak growth occurs for middle wavelengths ($k=4$–10) increases with phase shift (rm) of the IC: $t\sim 0$ for rm = 1; $t=0.5$ d for rm = 1.5; $t\sim 1$–1.5 d for rm = 2. For short wavelengths ($k > 12$), the change in initial phase shift only slightly alters the time of peak growth ($t\sim 0$–0.5 d). And, somewhat opposite to the longer waves, the peak value for rm = 1.5 is less than that for rm = 2 and more than that for rm = 1. The peak value is 2–3 times the asymptote for the shortest waves. The asymptotic values are reached more rapidly for the middle wavelengths (~4 d for $k=4$ through 8). For shorter waves, the time to reach the asymptote takes progressively longer and exceeds 10 d for wavenumbers $k > 16$.

The separated case results (Fig. 3b) are similar to those for the connected IC after 4 days, but very different during the first two days. The ratio of peak to asymptotic growth rate (GRR) is again larger for shorter than middle waves, but that ratio (GRR ~1.1–1.6) is much less than in the connected case. Curiously, the growth rate values and evolution are very similar for a wide range of waves ($7<k<16$) during days 1 and 2 for rm = 1.5. Unlike the connected cases, there is no tendency for the peak growth rate to increase with k for shorter waves. Also contrary to the connected IC cases, peak values occur for middle waves ($k\sim 10$ for rm = 1.5; $k\sim 8$–10 for rm = 1 and 0.5). These peak values are much less than in the connected case. For middle waves, the peak values only slightly exceed (by < 2%) the asymptotic values. These peak values are reached later for rm = 0.5 than for rm = 1. The growth rate at the start is

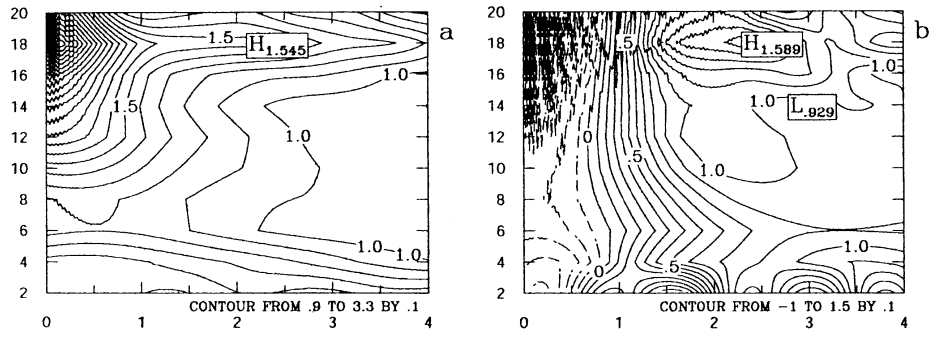

FIGURE 3 Time series of total energy growth rate ratio (GRR). The abscissa is time in days; the ordinate is zonal wavenumber. The actual growth rate for wavenumbers $k=2$–10 may be obtained by multiplying the normalized value shown here by the corresponding value for UMR = 1 in Figure 2a. For waves shorter than $k=10$, the instantaneous growth rate was normalized by the value after 10 days. Dashed lines indicate negative values. Both (a) connected and (b) separated IC use rm = 1.5.

TABLE I Normalized projections onto symmetric modes at $k = 8$. The nine largest modes are shown for the separated initial conditions (IC). The five largest modes are shown for the connected IC. Mode UMR = 128 is the most rapidly decaying mode, complementary to the MUNM: UMR = 1. Mode UMR = 2 has complement 127, similar pairs are: UMR = 3 with 126; UMR = 16 with 114. CM is a neutral continuum mode

		Separated Case				*Connected Case*		
UMR	*Phase Speed*	*rm = 1 IC (t = 0)*	*rm = 1.5 IC (t = 0)*	*rm = 1.5 t = 2.5 days*	*rm = 1.5 t = 5 days*	*rm = 1.5 IC (t = 0)*	*rm = 1.5 t = 2.5 days*	*rm = 1.5 t = 5 days*
1	0.024	0.893	0.745	1.000	1.000	0.833	1.000	1.000
2	0.021	1.000	1.000	0.784	0.457	1.000	0.701	0.408
3	0.018	0.774	0.811	0.482	0.214	0.739	0.393	0.175
16	0.015	0.615	0.693	0.212	0.049	0.393	0.108	0.026
CM	0.014	1.102	1.175	0.356	0.081	0.763	0.207	0.047
114	0.015	0.639	0.699	0.212	0.049	0.383	0.104	0.025
126	0.018	0.770	0.856	0.132	0.015			
127	0.021	1.061	1.111	0.130	0.013			
128	0.024	0.894	0.962	0.066	0.003			

negative for all wavenumbers when rm = 1.5, while it is near zero for all wavenumbers when rm = 1. (For very high wavenumbers, $k \sim 17$–20, growth rates are negative at $t \sim 0.5$–1 d.)

Analysis in Cartesian geometry (Hodyss and Grotjahn, 2002) finds similar negative growth rates; in that geometry they result in part from rapidly decaying normal modes that have much larger amplitude in the separated IC for rm = 1.5 than do the growing modes. Projections onto the IC (Table I) reveal a different explanation in spherical geometry. For the separated case (rm = 1.5) the top nine projections include the three most rapidly growing and the three most rapidly decaying normal modes. The presence of these three modes UMR = 1, 2, and 3 might be anticipated from their structure. Considering first the meridional profile, the MUNM has a single peak like the IC do, but it is centered near 37°N for the MUNM and 30°N for the IC. As mentioned, UMR = 2 is dipolar in the meridional with a larger peak near 30°N than the complement near 43°N. UMR = 3 is tripolar with largest extrema near 30°N and others at 40 and 49°N. The higher UMR are more bottom trapped, hence, combining them in a way to create a primary wavetrain near 30°N at upper levels will result in several significant wavetrains at low levels. That excess is greatly reduced by the largest neutral mode (labeled CM) present. CM is strongly bottom trapped and has its two primary wavetrains centered near 35 and 43°N. Unlike the Cartesian geometry, the decaying modes are comparable to the growing ones for the separated IC. If the solution were to contain only the growing mode and its decaying "mate" then initially the growth rate would be zero; then, the growth rate would ramp up to the growing mode rate over time. Since the two members have similar amplitude for each growing/decaying pair of eigenmodes in this IC, the early *negative growth rates of the separated IC cases must be coming from an NG process.* (This is easily demonstrated by a simple analogy. If the growing and decaying pair are modeled by $f(t) = \exp(t) + \exp(-t)$, then $df/dt = 0$ at $t = 0$ and is positive thereafter.) In contrast, for the connected case, the top four projections (Table I) include the top three most rapidly growing modes, but *not* the associated decaying modes. Those decaying modes have much smaller amplitude (by at least a factor of 10) in the connected IC. Consequently, while the NG process is no doubt operating, it is clear from the projection magnitudes that UNMG is also strongly contributing to the large early growth.

3.4. KE/APE Ratio

TE has two components (KE and APE). To assess the relative contributions of the two components to TE, the ratio KE/APE is used. Generally this ratio increases with zonal wavenumber for both IC. The ratio of KE/APE evolves differently for the two IC even though the asymptote must be the same (~ 0.6 for $k > 8$). KE dominates the total energy for the shorter waves, during the first day or so. Hence the TE growth rate time series of short waves will be heavily influenced by the KE growth rates.

For the connected ICs and short waves ($k > 11$) the ratio peaks at a time that varies with the upstream tilt: $t \sim 0.6$–1.5 d for rm $= 2$; $t \sim 0.4$–1.0 d for rm $= 1.5$; $t \sim 0.2$–0.5 d from rm $= 1$. The peak value of the ratio is least for the largest of these three rm values and *vice versa*. For example, at $k = 12$, the peak ratio is: 1.4 at rm $= 1$; 1.1 at rm $= 1.5$, and 1.0 at rm $= 2$.

In the separate IC, APE $\sim$ KE for the middle waves but APE is much less for the short waves. KE/APE exceeds 3 where $k > 11$ in this IC. The ratio remains higher for a longer time in the rm $= 1$ than in the rm $= 1.5$ or rm $= 0.5$ separated IC. This result is partly a property of using wavetrains at upper and lower levels. Increasing the phase shift from rm $= 1$ (one half wavelength) to rm $= 2$ in the separated IC makes an upper trough seem to be less and less downstream instead of further upstream from the nearest surface trough. A zonally-localized trough might show a trend with increasing upstream phase shift similar to that found for the connected IC and for positive rm < 1 in the separated IC.

3.5. Amplitude and Kinetic Energy

In Cartesian geometry, KE has identical growth rates as squared amplitude (L2) for plane and square wave solutions. For meridionally localized solutions L2 is quite similar to KE in Cartesian simulations by Hodyss and Grotjahn (2002). For all the calculations discussed for this model, KE growth rates are similar enough to the L2 growth rates so that KE can also be used to describe general properties of amplitude growth.

For the connected cases, the peak KE growth rates exceed the asymptotic values at every wavenumber (Fig. 4a). The ratio of peak/asymptote growth rate is GRR ~ 1.5–2

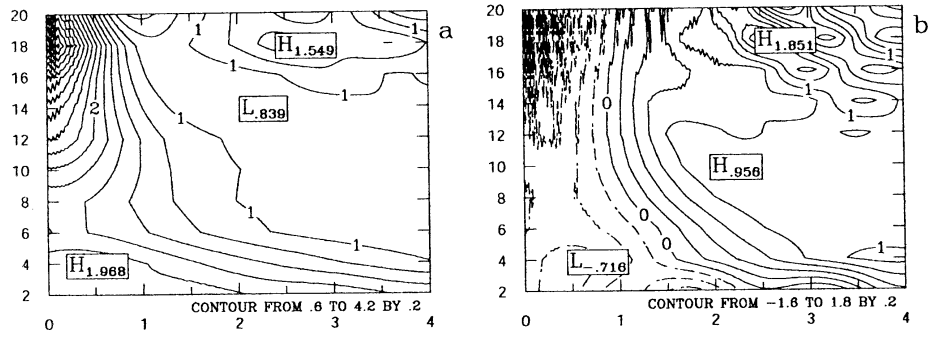

FIGURE 4 Similar to Figure 3 except for kinetic energy.

for most of the middle wavenumbers ($k \sim 6$–10) and the time of peak occurrence is later for: longer wavelengths and larger initial upstream tilt. For the shorter waves ($k > 12$) the peak/asymptote value exceeds 3 for many waves and occurs within the first day. Hence, NG is briefly quite a strong mechanism that increases for increased tilt qualitatively in agreement with Cartesian results.

For the separated cases (Fig. 4b) the KE growth rate is small or negative early on. For rm = 1.5 the values are negative for all k during the first day. For "less" phase shift (rm = 1) negative growth rates only occur for $k > 14$ during the latter half of the first day. For rm = 0.5 negative growth also occurs in the latter half of day 1, but for $k > 8$. Since the KE/APE ratio was significantly greater than one in these IC, similar negative growth rates were seen in total energy. The negative values occur later for rm = 1 than rm = 1.5 – opposite to the timing change seen for the connected IC. Shorter wave results for rm = 0.5 are very similar to rm = 1 results. For some middle and all short wavelengths shown, the growth rate never exceeds the asymptotic value. At other middle wavenumbers ($k = 8$–10) by $t \sim 2.0$ growth rates approach 85–95% of the asymptotic value; for rm = 0.5, growth rates do not reach 85% of the asymptote until $t \sim 3.0$. APE growth rates also peak near these times and thus total energy also has a maximum at this time. Hence, NG is not a strong effect, again in qualitative agreement with Cartesian results for amplitude as well as KE.

3.6. Available Potential Energy

For the connected cases, the time series (Fig. 5a) of APE growth rate are remarkably flat for the long and middle wavelengths; at $k = 6$–8 the growth rates are almost immediately the asymptotic value. Since the IC is dominated by the three most unstable normal modes at $k = 8$ (and their decaying counterparts are much smaller amplitude) UNMG can explain much of the pattern seen. Since GRR slightly exceeds 1.0 early on for this IC, the NG mechanism provides some growth. For this IC it was found that NG strongly amplified the KE growth rate but that is not the case for APE. Examination of the KE and APE distributions for the top five projections can explain this difference. The key difference lies in the meridional profiles. APE for all these modes has much greater meridional confinement than does KE. Consequently, the

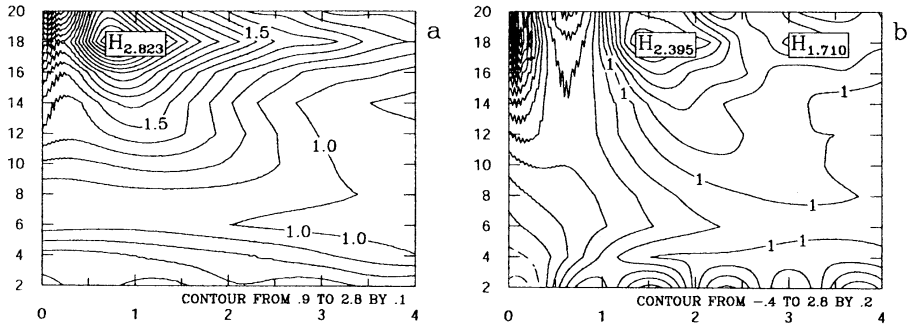

FIGURE 5 Similar to Figure 3 except for available potential energy.

overlap between the different modes is much smaller for APE than KE. Since there is less overlap, the constructive/destructive interference between modes (present in NG) is less for APE than for KE. Another difference is that the APE fields are strongly bottom trapped, whereas the KE fields for the four growing modes have significant amplitude through the troposphere. Analogous solutions in Cartesian geometry show similar nearly constant growth rate. For $k > 6$, the peak value of GRR increases with k. These shorter waves ($k \sim 10$–20) have an oscillatory time series during the first day: where the peak values occur at later times (0.5–1 day) for greater initial upstream tilt. A relative minimum in growth rate occurs about a half day earlier than this peak. This relative minimum still exceeds the asymptotic value for most short waves in the three phase shifts considered. A similar oscillation is seen in analogous Cartesian geometry results.

For the separated cases, the peak values of APE growth rates (Fig. 5b) do not exceed the asymptote for $k < 8$. Further, the growth rates start very small (or negative) and slowly 'ramp up' to the asymptotic value, an evolution consistent with little NG occurring. For very short waves ($k \sim 16$–20) growth rates exceed the asymptote by at least 50% during days 1–3; with some tendency for growth to exceed the asymptote earlier for less upstream phase shift in the IC. There is an oscillation in the growth rates of the shortest waves ($k \sim 14$–20) though it is more prominent than for the connected IC. Negative growth rates occur near the start for rm = 1 and 0.5; but an analogous relative minimum occurs a half day later for rm = 1.5 As noted in the KE/APE ratio and the KE data, the pattern for the shortest waves occurs later in time for "less" upstream tilt – the opposite to the connected IC. As already noted, this property arises from using wavetrains instead of single upper and lower troughs.

3.7. Potential Enstrophy Growth Rates

For the connected cases the peak/asymptotic value exceeds 1.2 for $k \sim 12$–20 in all three phase shifts tested. This ratio increases with wavenumber and exceeds 2 for $k > 16$. For most middle and longer waves ($k = 2$–6) the growth rates are remarkably flat (similar to the APE growth rates for the corresponding integrations). Hence, GRR ≤ 1.1 for $k = 2$–8. As with APE, NG is initially comparable to UNMG but its share declines over time somewhat matching the increasing normal mode component of the total growth. Also similar to the energy components, the ratio GRR increases with k for short waves ($k > 10$).

For the separated cases, the growth rates start below or near zero and rapidly increase during the first day. A peak value is reached between days 1 and 2 (sooner for shorter zonal wavelengths); the peak value of GRR exceeds 1.5 for wavenumbers $k > 10$. Similar to Cartesian geometry results, the peak growth rates of H occur for much longer waves in this IC than for the connected IC. However, peak GRR values again occur for the shortest wavelengths. Unlike the energy components, peak GRR values for middle waves are more similar to the connected IC values. In Cartesian geometry, greater NG was also found for H than energy components and the larger GRR values are similar to the largest found here. In Grotjahn and Hodyss (2002) the amount of NG in H near the start depended strongly on the initial boundary PV and that boundary PV was in turn very sensitive to adjustments in perturbation structure at the bottom.

4. CONCLUSIONS

The relative importance of NG and UNMG was considered in spherical geometry. Two different types of ICs were studied: a "connected" vertical structure and a "separated" vertical structure. The connected IC relates to ICs commonly used in most prior work in Cartesian geometry. The separate IC is intended to approximate conditions prior to observed cyclogenesis (e.g., Grotjahn, 1996). The connected IC develops large NG in Cartesian models, especially simpler models like Eady's. In spherical geometry it again develops more NG than the "realistic" IC studied.

The relative presence of NG or UNMG is identified using time series of the growth rates in conjunction with eigenmode projections. Growth rates considered were amplitude squared (L2), mass-integrated energy (TE and its components KE and APE) and potential enstrophy (H). The relative amounts of NG were estimated in this general way because of a large difference between the first and second most unstable modes (UMR = 1 and 2) for the wavelengths of most interest. This difference was less pronounced for weaker basics state jets. Projecting the total solution upon the complete set of corresponding eigenvectors found that the three most unstable normal modes (at a given k) were prominent in both ICs. For the separated IC, the corresponding three most highly damped normal modes were also prominent, but not so in the connected IC. The strongly damped normal modes tended to cancel the growing modes very early in the integration of the separated case. Since the damped modes played little role in the connected IC case, a general result was that UNMG was much stronger early on ($t < 2$ days). The projections also proved that negative growth of some variables for the separated IC early on had to be due to the NG mechanism. For the connected case, the NG and UNMG mechanisms were both positive. The projections also showed a general result that amplitude, KE, and H would be likely to have more NG then APE because the latter field has less overlap between modes than the former fields.

Some specific results are as follows. The peak TE growth rate increases with wavenumber for both IC, hence NG increases greatly with wavenumber. The peak value is typically 2–3 times the asymptote for the shortest waves in the connected IC. The separated IC results are similar to those for the connected IC after four days, but very different during the first two days. By four days, the growing normal modes dominate the solution (Table I). The ratio of peak to asymptotic growth rate (GRR) is again larger for shorter than middle waves, but that ratio (GRR $\sim$ 1.1–1.6) is much less than in the connected case. During the first two days, NG is significant and positive for the connected IC cases but negative for the separated IC cases.

KE is the dominant part of the total energy for the shorter waves during the first day or so. Hence the TE and KE growth rate time series for short waves were very similar during the first two days. For all the calculations discussed for this model, KE growth rates were similar enough to the L2 growth rates so that KE was also used to describe general properties of amplitude growth. For the connected IC, NG was briefly quite a strong mechanism that increases for increased initial tilt qualitatively in agreement with Cartesian results. In contrast, for the separated IC the NG mechanism was weak or negative, so that the growth rate never exceeds the asymptotic value in some middle and all low wavenumbers shown.

Both NG and UNMG have made comparable contributions to the pattern seen in APE growth rates for the connected IC. The NG mechanism is not as strong for APE as it was for KE. Examination of the KE and APE distributions for the top

five projections shows that KE for all these modes has much greater meridional spread than does APE. Since there is less overlap of APE than KE, there is less interference between modes and the amount of NG is less for APE than for KE. For the separated IC cases, the APE growth rates start very small (or negative) and slowly 'ramp up' to the asymptotic value, an evolution consistent with the emergence of an unstable normal mode, the reduction of initially comparable complementary decaying normal modes, and little NG occurring (from similar phase speeds of the primary modes present).

A drawback of the separated IC is the use of wavetrains at upper and lower levels. One may speculate about what would happen when using horizontally localized structures in the IC. The phase speed for an unstable mode of a given UMR is nearly constant with wavenumber. This result could allow localized structures, based on combining the MUNMs at many wavenumbers, to remain coherent for several days and thus allow little NG once the MUNM combination emerges from a more general initial state.

Acknowledgments

This work was supported in part by grants from the National Science Foundation (ATM 96-15316) and the University of California, Davis.

References

Badger, J. and Hoskins, B.J., "Simple initial value problems and mechanisms for baroclinic growth", *J. Atmos. Sci.* **58**, 38–49 (2001).
Eady, E., "Long waves and cyclone waves", *Tellus* **1**, 33–52 (1949).
Farrell, B., "Modal and nonmodal baroclinic waves", *J. Atmos. Sci.* **41**, 668–673 (1984).
Farrell, B., "Optimal excitation of baroclinic waves", *J. Atmos. Sci.* **46**, 1193–1206 (1989).
Frederiksen, J., "Growth rates and phase speeds of baroclinic waves in multi-level models on a sphere", *J. Atmos. Sci.* **35**, 1816–1826 (1978).
Grotjahn, R., "Composite trough evolution of selected west Pacific extratropical cyclones", *Mon. Wea. Rev.* **124**, 1470–1479 (1996).
Grotjahn, R. and Castello, C., "A study of frontal cyclone surface and 300-hPa geostrophic kinetic energy distribution and scale change", *Mon. Wea. Rev.* **128**, 2865–2875 (2000).
Grotjahn, R. and Tribbia, J., "On the mechanism of cyclogenesis as deduced from vertical axis tilts", *Tellus* **47A**, 629–637 (1995).
Grotjahn, R., Hodyss, D. and Immel, S., "A technique for creating linearly stable localized atmospheric features with an application to nonlinear cyclogenesis". Submitted to *Dyn. Atmos. Ocn* (2002).
Grotjahn, R., Pedersen, R. and Tribbia, J., "Linear instability with Ekman and interior friction. Part II: initial value analysis", *J. Atmos. Sci.* **52**, 764–777 (1995).
Hodyss, D. and Grotjahn, R., "Diagnosing cyclogenesis by partitioning energy and potential enstrophy in a linear quasi-geostrophic model", *Tellus* **53A**, 567–577 (2001).
Hodyss, D. and Grotjahn, R., "Nonmodal and unstable normal mode baroclinic growth as a function of horizontal scale". Submitted to *Dyn. Atmos. Ocn* (2002).
Hollingsworth, A., Simmons, A. and Hoskins, B., "The effect of spherical geometry on momentum transports in simple baroclinic flows", *Quart. J. Roy. Meteor. Sci.* **102**, 901–911 (1976).
O'Brien, E., "Optimal growth rates in the quasigeostrophic initial value problem", *J. Atmos. Sci.* **49**, 1557–1571 (1992).
Petterssen, S. and Smebye, S., "On the development of extratropical cyclones", *Quart. J. Roy. Meteo. Soc.* **97**, 457–482 (1971).
Rotunno, R. and Fantini, M., "Pettersen's type B cyclogenesis in terms of discrete, neutral Eady modes", *J. Atmos. Sci.* **46**, 3599–3604 (1989).
Rotunno, R. and Bao, J.-W., "A case study of cyclogenesis using a model hierarchy. *Mon. Wea. Rev.* **124**, 1051–1066 (1996).

Simmons, A. and Hoskins, B., "Baroclinic instability on the sphere: normal modes of the primitive and quasi-geostrophic equations", *J. Atmos. Sci.* **33**, 1454–1477 (1976).
Simmons, A. and Hoskins, B., "The downstream and upstream development of unstable baroclinic waves", *J. Atmos. Sci.* **36**, 1239–1254 (1979).
Whitaker, J. and Barcilon, A., "Type B cyclogenesis in a zonally varying flow", *J. Atmos. Sci.*, **49**, 1877–1892 (1992).

APPENDIX

Abbreviations

APE	global mass-weighted integral of quasi-geostrophic available potential energy.
GRR	growth rates ratio: instantaneous value over the asymptotic value at a given k
H	global mass-weighted integral of squared quasi-geostrophic potential vorticity
IC	initial condition
k	zonal wavenumber
KE	global mass-weighted integral of quasi-geostrophic kinetic energy
L2	global mass-weighted integral of squared amplitude
MUNM	most unstable normal mode at a given k
NG	nonmodal growth, a mechanism having increasingly favorable superposition of eigenmodes
rm	measure of upstream phase shift. rm = 1 is 1/2 wavelength shift from the surface to 200 hPa. (i.e. a trough at 200 hPa overlies the surface ridge)
TE	global mass-weighted integral of total energy: KE + APE
UMR	unstable mode rank at a given k (i.e. UMR = 1 is the MUNM, = 2 the second most unstable, etc.) of equatorially symmetric modes
UNMG	linear growth mechanism as found for normal unstable modes